

# HOM-MITIGATION FOR FUTURE SPS 33-CELL 200 MHz ACCELERATING STRUCTURES

P. Kramer<sup>1\*</sup>, C. Vollinger, CERN, Geneva, Switzerland

<sup>1</sup>also at Institute of High Frequency Technology (IHF), RWTH Aachen University, Germany

## Abstract

The CERN SPS 200 MHz travelling wave (TW) accelerating structures pose an intensity limitation for the planned High Luminosity (HL-) LHC upgrade. Higher-order modes (HOMs) around 630 MHz have been identified as one of the main sources of longitudinal multi-bunch instabilities. Improved mitigation of these HOMs with respect to today's HOM-damping scheme is therefore an essential part of the LHC injectors upgrade (LIU) project.

The basic principles of HOM-couplers in cavities and today's damping scheme are reviewed, before illustrating the numerous requirements an improved damping scheme for the future 33-cell structures must fulfil. These are, amongst others, the mitigation of HOMs situated in the lower part of the structure where there are no access ports for extraction, a sufficient overall damping performance and an acceptable influence on the fundamental accelerating passband (FPB). Different approaches tackling these challenges are investigated and their performance, advantages and pitfalls are evaluated by ACE3P and CST electromagnetic (EM) field solver suites.

## INTRODUCTION

The Super Proton Synchrotron (SPS) at CERN relies on a 200 MHz multi-cell travelling-wave structure (TWS) for particle acceleration.

Beam dynamic simulations showed that to achieve stable beams for future HL-LHC intensities an additional mitigation by a further factor three of already heavily damped HOMs around 630 MHz is necessary in these structures [1]. A general overview of the SPS accelerating structure and the corresponding longitudinal and transverse HOM damping schemes in use today were presented in [2, 3]. For beam loading reasons, shorter 33-cell structures will be employed after the LIU upgrade together with the 44-cell structures in use today. The longitudinal damping scheme deployed today on 44- and 55-cell structures is insufficient for the HOMs around 630 MHz with future beam intensities. This equally applies if this damping scheme is used on the 33-cell structures (shown as black HOM-couplers in Fig. 1).

\* patrick.kramer@cern.ch

As outlined in [3], these couplers were optimized on a single 11-cell section featuring HOMs with an integer multiple of a  $\pi/11$  phase advance per cell. One such spare section is shown in Fig. 2. On 33-cells, HOMs with phase advances



Figure 2: 11-cell section of the accelerating TWS.

that are not allowed on 11-cells exist and the performance of the HOM-coupler on these modes has to be verified.

To achieve the required additional damping by a factor three of the HOMs around 630 MHz this contribution describes the systematic improvement of the existing damping scheme. The resulting beam impedance is thereby calculated by time domain wakefield simulations. Due to the importance of the damping upgrade for the future operation of the SPS, confirmation of the results by two different solver types was desired. The finite-difference wakefield solver of the CST suite [4] and the finite-element time domain solver (T3P) of the ACE3P [5] suite were used for this purpose.

The first section of this work details the model set-up and the simulation settings used for the two solvers. The HOM-mitigation strategy then comprises the following steps. First, additional couplers are placed in cells with strong electric field of the most dangerous modes present in the 33-cell configuration. These modes feature a high geometry factor R/Q. As a second step, the HOM-coupler is optimized to reach close-to-critical coupling to the HOMs in the relevant frequency range. Sufficient damping can however not be achieved merely by adding HOM-couplers in the available access ports at the top of each cell (Fig. 2). This is due to the fact that the top/ bottom symmetry of the structure is violated and as a result the EM fields of some modes are partially pushed towards the lower half of the cavity where no dedicated access ports are available for HOM-damping (for more details see [3] and compare Fig. 8a later in the text). One particular example for this effect is the high-Q  $17\pi/33$  mode. Several means of damping modes in the lower half

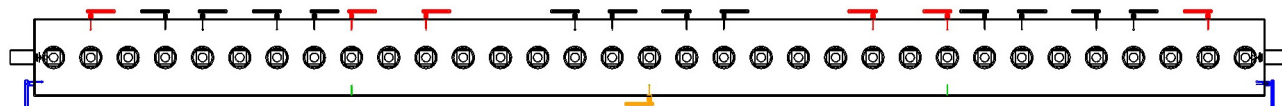


Figure 1: Several HOM-mitigation options shown together in a 3-section model. Black: existing longitudinal damping scheme. Red: additional couplers. Blue: end-plate couplers. Orange: VPP coupler. Green: mitigation by resonant posts.

Content from this work may be used under the terms of the CC BY 3.0 licence (© 2018). Any distribution of this work must maintain attribution to the author(s), title of the work, publisher, and DOI.

of the structure are therefore studied as a third step. Finally, a new principle of HOM mitigation by introducing slight structural changes via resonant posts was developed and is demonstrated. This way, machining of cavity parts that could pose a potential integrity risk could be avoided. The task of finding a satisfactory mitigation scheme is aggravated even further by the fact that the FPB may merely be influenced to a very small extent by couplers and posts and in addition some access ports are needed for transverse impedance damping.

## WAKEFIELD CALCULATIONS

Although particle acceleration is performed via a travelling wave FPB, the HOMs up to 1.3 GHz are of standing wave type. The fundamental power couplers (FPCs) couple merely very narrowband to some frequencies in the 630 MHz range. Due to modifications in the TWS's amplifiers, the FPCs situated in the end-cells of the accelerating structure (Fig. 1) are currently redesigned and their final configuration is not yet decided. With this comes uncertainty in how much the EM fields are perturbed by the presence of the FPCs and uncertainty in the amount of their coupling to and consequently damping of the HOMs. In addition, the impact of the final matching networks attached to the FPCs for the travelling-wave FPB on the HOMs remains undefined to date. The process of finding a sufficient damping scheme was therefore carried out by assuming the worst case of no coupling of the FPCs to the HOMs. The FPCs must be included in the model to obtain the appropriate field profiles due to their presence in the end-cells. However, they are short-circuited in the plane of the end-plates which then results in full reflection of any HOM power picked up by the FPCs, see Fig. 3a. To obtain the beam impedance for the FPB of course another wakefield simulation has to be conducted with the appropriate matching networks for the travelling-wave condition attached [6].

At present, the HOMs of the structure are only of interest up to a frequency of 1 GHz. In T3P the tank volume can then be meshed quite coarse (Fig. 3a) as curved tetrahedral elements are used that are however not visualized in Fig. 3. The electric pick-ups have to be meshed densely and the superiority of a tetrahedral over a hexahedral mesh in modelling the fine structures and making a smooth transition to the large tank volume is evident when comparing the meshes shown in Figs. 3b and 3c. Mesh and time step convergence studies were conducted and led to the final simulation settings given in Table 1. A magnetic boundary condition at the vertical symmetry plane ( $x=0$ ) was used. For details about the calculation methods used in T3P refer to [7].

The results for the impedance of HOMs in the harmful 630 MHz range of a 33-cell structure with today's damping scheme are shown in Fig. 4a. In addition to a discrepancy in frequency, the results obtained from the two solvers also differ significantly in at least one of the impedance peaks. The calculated longitudinal impedance of around 100 kΩ for the 33-cell structures is too high for HL-LHC beam

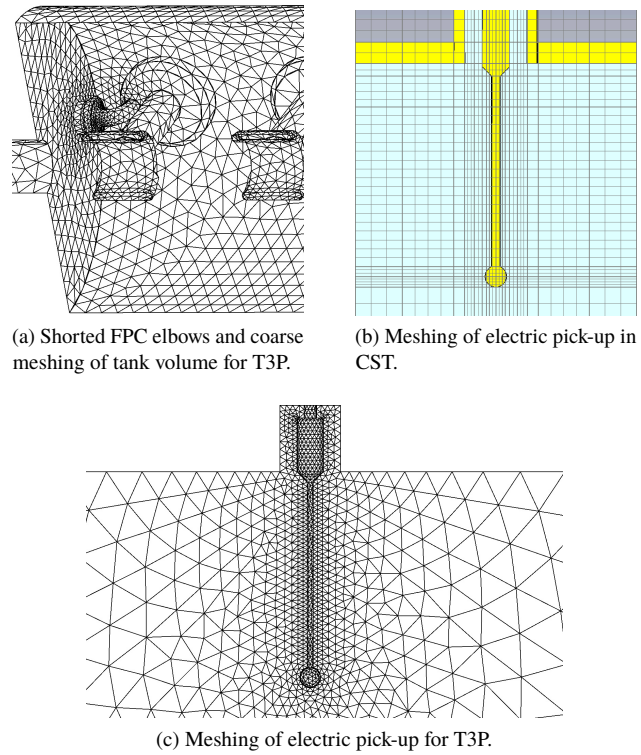


Figure 3: Discretization of the computation domain with tetrahedra for T3P and hexahedra in CST.

Table 1: Simulation Settings in T3P and CST Respectively

Parameter	T3P	CST
$f_{\max}$ [GHz]	1	1
bunch $\sigma_z$ [cm]	11.5	10
# mesh [Mio.]	1.2 - 1.4 tets	16 - 21 hex
$\Delta t$ [ps]	24	$\sim \approx 1.3$
wake [km]	2/1.5	3
basis order	2	-
linear solver	MUMPS	-

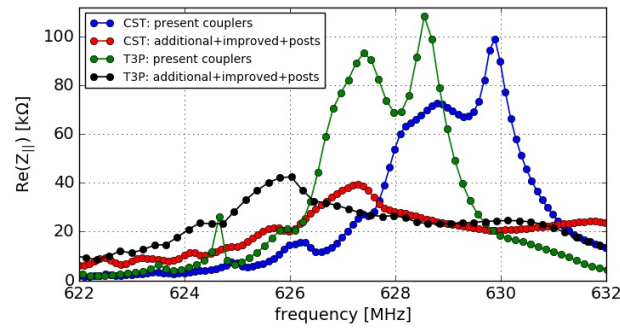
intensities. Several methods to mitigate this impedance are outlined in the following.

### STEP 1: ADDITIONAL HOM-COUPLERS

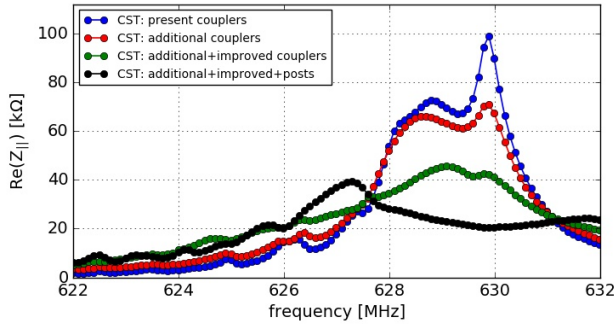
To further damp the two high-R/Q HOMs with  $14\pi/33$  and  $15\pi/33$  phase advance that exist in the 630 MHz frequency band, additional couplers should be put in cells where these two modes feature strong electric field. In this respect, the eigenvector solutions of a coupled resonator chain, as for example outlined in [8], can be used to obtain relative electric field strengths in the centre of each cell:

$$\xi(m, j) = \sqrt{\frac{2 - \delta_{mN}}{N}} \sin \left[ m\pi \left( \frac{2j - 1}{2N} \right) \right] \quad (1)$$

in cell  $j = 1, \dots, N$  for mode  $m = 1, \dots, N$ ,  $N$  being the total number of cells and  $\delta_{mN}$  the Kronecker delta. The eigenvalue solutions of the equation system generated by the simple resonator chain with nearest neighbour coupling are unable



(a) Comparison of CST and T3P impedance results.



(b) Damping improvement due to the different mitigation techniques.

Figure 4: Simulated longitudinal beam impedance in the 630 MHz range for the different HOM mitigation schemes calculated by the two EM solvers.

to predict mode frequencies or model the passband of the HOMs. However, when comparing to 3D EM field solver solutions the eigenvectors proved to predict the relative electric field amplitudes very well even for cases with a high number of HOM-couplers. Figure 5 shows the normalized mode amplitudes for the three most problematic modes in a 33-cell structure. For better readability and symmetry reasons, the amplitudes are plotted for the first 17 cells only. It

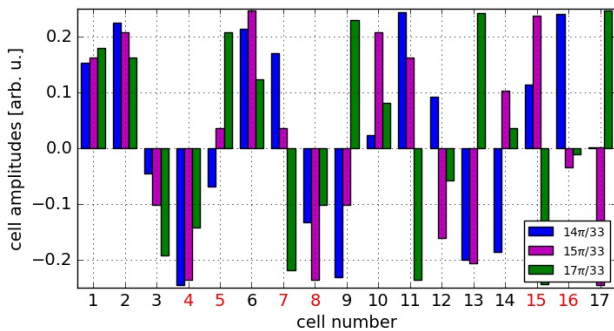


Figure 5: Mode amplitudes following Eq. (1) in the centre of cells for the three most problematic HOMs. Only the  $14\pi/33$ -mode is antisymmetric to cell 17. Red labels mark cells already occupied by today's damping scheme.

is obvious that some of the HOM-couplers in the present damping scheme can contribute well to the damping of the high-R/Q modes. Ideally, additional couplers would now be put in cells with strong electric field of both high-R/Q

modes. As few couplers as possible should be used to avoid that the energy of the HOMs is stored mostly in the lower half of the cavity. This effect will also be taken care of in steps three and four below. Unfortunately the obvious choice of cell six can not be used, as five consecutive couplers push some modes in-between cells, i.e. an area inaccessible for the couplers. After carefully analysing Fig. 5 and confirming with only a few full model simulations, overall optimal results are found by adding six additional couplers drawn in red in Fig. 1. Table 2 shows characteristics of the three modes of concern for this case of additional couplers as obtained from Eigenmode simulations. Comparing the values

Table 2: Characteristics of the Three Most Deteriorating HOMs in a 33-cell Structure for the Cases Illustrated in Fig. 1

	$f$ [MHz]	$Q$	$R/Q$ [ $\Omega$ ]	$R$ [k $\Omega$ ]	$\phi$ [rad]
additional	627.7	8450	7.4	62.5	$17\pi/33$
top-	629.3	281	85	23.9	$15\pi/33$
couplers	630.4	195	123	24.0	$14\pi/33$
end-plate	627.6	2183	9.5	20.7	$17\pi/33$
coupler	629.4	360	75	27.0	$15\pi/33$
	630.4	199	116	23.1	$14\pi/33$
pedestal	627.7	2070	10.4	21.5	$17\pi/33$
coupler	629.2	250	86	21.5	$15\pi/33$
	630.3	195	124	24.2	$14\pi/33$
VPP	627.7	3642	1.5	5.5	$17\pi/33$
coupler	629.3	262	79	20.7	$15\pi/33$
	630.3	194	123	23.9	$14\pi/33$
VPP	627.7	3683	1.5	5.5	$17\pi/33$
mitigation	628.2	271	55	14.9	$15\pi/33$
	630.0	233	94	21.9	$14\pi/33$

with those given in [3] for today's damping scheme, we draw two conclusions. First, the  $Q$  of the  $17\pi/33$ -mode is vastly increased and second, the impedance of the two high-R/Q modes is essentially halved despite the fact that their quality factors are already quite low in today's configuration. The wakefield result for this case is shown in Fig. 4b.

## STEP 2: HOM-COUPLER IMPROVEMENT

The existing 630 MHz coupler was deployed in the first year of SPS operation (1976) and shows very good damping performance [3]. If possible, the coupler must however be further optimized to achieve the required additional damping. The fundamental coupler theory is therefore briefly reviewed on a single-cell cavity in the following. In the circuit of Fig. 6 the cavity is modelled by the parallel  $RLC$  resonator and the electric pick-up by the capacitance  $C_e$ . The parasitic stray capacitance of the probe-tip due to fringe fields is modelled by the capacitance  $C_s$  to ground. For a purely resistive load it can easily be shown that the maximum obtainable damping is limited by the stray capacitance  $C_s$ , as it partially shunts the displacement current picked up by the probe [9]. This can

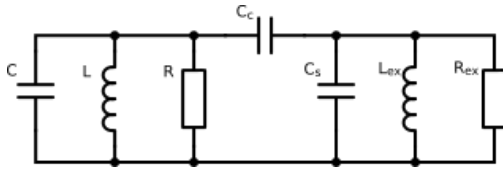


Figure 6: Electric coupling of a resistive ( $L_{ex} = 0$ ) or complex load to a single-cell cavity.

be circumvented at a single frequency by compensating the stray capacitance with an inductance  $L_{ex}$ , thereby forming a second resonant circuit. As cavity and coupler now behave as two electrically coupled resonant circuits, the achievable damping is limited by the load  $R_{ex} = R_{crit}$  for which critical coupling occurs [10]. For  $R_{ex} < R_{crit}$  the cavity resonance is split in two impedance peaks.

Due to the dimensions of the electric probe of the existing HOM-coupler with a length of  $l \approx 105 \text{ mm} \approx \lambda/4$  the probe and therefore the coupler are already resonant around 630 MHz and above described resonant effects occur even without the deployment of a complex load. Consequently, a very good performance of the coaxial coupler can be achieved even if it is merely terminated with its characteristic impedance of  $R_{ex} = 50 \Omega$ . The choice of coupler and load impedance is however not optimal as cavity and coupler are not close-to-critically coupled as shown in Table 3. Eigenmode simulations of a single cell with periodic

Table 3: Coupling to the Two High-R/Q Modes on a Single Cell (SC)

	$5\pi/11$		$14\pi/33$	
	f [MHz]	R [ $\Omega$ ]	f [MHz]	R [ $\Omega$ ]
SC	628.9	340k	629.6	330k
SC+50 $\Omega$ -coupler	628.7	956	629.4	1074
SC+23 $\Omega$ -coupler	624.1	270	626.0	295
	633.1	556	635.6	214

boundaries and loaded by one HOM-coupler show under-critically coupled behaviour for an impedance of  $50 \Omega$  (as the frequency is merely slightly perturbed by the presence of the coupler). An impedance of  $23 \Omega$  however leads to the splitting of the cavity mode into two impedance peaks which are roughly leveled in amplitude for the  $14\pi/33$ -mode. The impedance of both high-R/Q modes is reduced and spread over a wider frequency range, see Table 3.

Due to the large number of couplers deployed today (72) and foreseen for the upgrade ( $\approx 120$ ) it is actually desirable to avoid a change of the coupler geometry. It is therefore investigated if improved damping can be achieved by deploying complex loads on the coupler output ports which are transformed by its  $50 \Omega$  transmission line to  $23 \Omega$  at the base of the probe. This implementation however will have a lower bandwidth than couplers with a  $23 \Omega$  characteristic impedance. A previous test consisted of equipping the

output ports of the couplers with complex conjugate matching networks in simulation for maximum power transfer of the HOMs to the loads. As the input impedances looking into the load ports of the couplers at the frequencies of the two high-R/Q HOMs lie clustered around  $(85-j35) \Omega$  on the Smith chart, the same matching network was applied on all couplers for simplicity. Note that this matching will in any case not be exact since cross-talk between the different couplers is not yet considered. The optimum is however considered to be flat and this rough test already resulted in a significant improvement of damping, see Fig. 4b. The effect that the impedance is increased below 627 MHz is likely due to the more narrowband behaviour of the complex loads. Compared to the  $23 \Omega$  suggested by the critical-coupling approach the impedance seen by the HOMs at the base of each probe is the complex load transformed by the 13 cm long transmission line of the coupler, which results in  $(24-j5) \Omega$ . So for this specific case complex conjugate matching and critical-coupling result roughly in the same complex load.

The final design and implementation of the complex loads are still under investigation and their verification by RF measurements is scheduled. It seems however unlikely that the future damping requirement can be met with additional and improved couplers alone. This is due to the high R/Qs of the HOMs involved but also due to the loss of top/bottom symmetry in the EM field patterns - problems which will be addressed in the next two sections.

### STEP 3: $17\pi/33$ -MODE MITIGATION

The  $17\pi/33$  mode is not being pushed into the lower part of the structure to such extreme extents with the FPCs in place. As the final redesign of the FPCs is not yet known, this mode is nevertheless used as an extreme case to study possibilities of damping modes that have most of their energy stored in the lower half of the structure.

#### End-plate Coupler

Only two access ports are available in the lower half of the cavity and they are situated on the end-plates, Fig. 1. These ports are already in use nowadays for damping of transverse impedance modes. As constraints on transverse impedance are less severe, one might however consider to use these ports for longitudinal damping instead. Taking again Fig. 5 into account, the EM field amplitude of the  $17\pi/33$ -mode is considerable in the end-cells. However, its electric field profile shown in Fig. 7a does not favour electric coupling. A probe reaching deep inside the end-cell close to the drift-tube appears infeasible since also the FPB features a strong electric field in this location. A probe shape as shown in Fig. 7b had therefore to be developed that is able to pull the field into the coaxial coupler. The existing filter part of the 630 MHz HOM-coupler was used during simulations due to its already good performance. Optimization of the probe dimensions is computationally expensive as due to the position of the coupler on the end-plates no single-cell approach can be used. Instead, at least half a 33-cell structure

Content from this work may be used under the terms of the CC BY 3.0 licence (© 2018). Any distribution of this work must maintain attribution to the author(s), title of the work, publisher, and DOI.

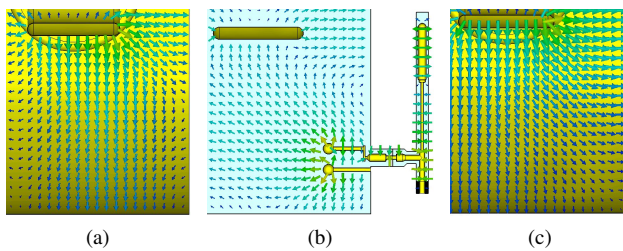


Figure 7: Electric field at end-plates of the  $17\pi/33$ -HOM (a,b) without and with coupler and of the FPB (c).

needs to be simulated by use of an H-symmetry plane in cell 17 to obtain the  $17\pi/33$ -mode. Table 2 exhibits the damping performance of the end-plate couplers on the high-Q mode and the slight detrimental effects on the  $15\pi/33$ -mode when used together with the additional top-couplers.

The end-plate coupler was found to induce a significant frequency shift of almost +100 kHz onto the FPB in standing mode. The reason for this is that the electric field of the FPB favours coupling to it from the end-plate ports, Fig. 7c. While the accelerating structure might be broadband enough to allow such a frequency shift, the notch filter of the coupler would need to handle an undesirable amount of power from the FPB.

### Pedestal Coupler

The electric field of the  $17\pi/33$ -mode is maximum in cell 17 as shown in Fig. 8a on the cross-section of this cell (cf. also Fig. 5). Another option to couple to this mode is in the areas surrounding the pedestals and an effective probe shape is shown in Fig. 8b. The bend vastly increases its coupling efficiency as the electric field is then orthogonally oriented on the probe tip. As observed in Fig. 8c the field profile of the FPB is not at all in favour of coupling to this probe shape and indeed no influence was observed in simulations. Deployment of this coupler would require

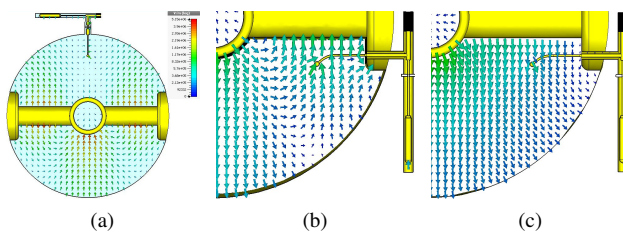


Figure 8: Electric field in cell 17 of (a)  $17\pi/33$ -mode (b) with pedestal coupler and (c) of accelerating mode.

machining or manufacturing a new drift-tube assembly per pedestal coupler (four 33-cell structures will be used after the LIU). Table 2 highlights the damping performance of a single pedestal coupler in cell 17 as a supplement to the existing and additional top-port couplers. The coupler can be conveniently optimized in simulations with an infinite periodic single-cell approach when the top-port coupler is also incorporated to create the  $17\pi/33$ -mode in the bottom of the cell.

### VPP Coupler

Three vacuum pumping ports (VPPs) are available underneath each 11-cell section (cf. Fig. 2) featuring a honeycomb grid in the inner copper layer with a hole diameter of 18.5 mm as shown in Fig. 9b. Not all pumping ports

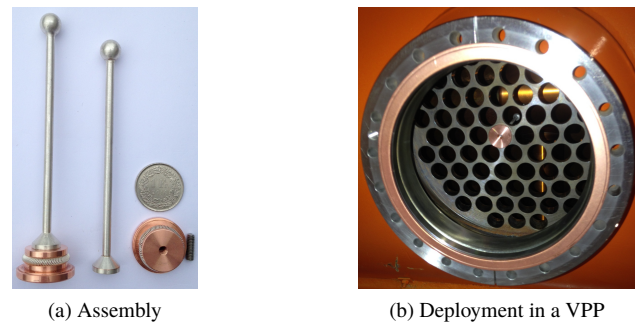


Figure 9: HOM-coupler pick-ups used as preliminary resonant posts.

are in use today nor is this so far planned for the future. Therefore, unused VPPs could be used as access ports for HOM-couplers in the lower half of the cavity. The use of one HOM-coupler in the centre cell that features strong electric field of the  $17\pi/33$ -mode is highlighted in Fig. 1 and its good performance, when used together with the additional top-port couplers, can be verified in Table 2. The coupler in the bottom of the cavity is highly effective for the mitigation of the  $17\pi/33$ -mode as not only its Q is damped but also its R/Q is vastly decreased, cf. Table 2. One can interpret that the electric field is pushed back up towards the top-couplers and the EM fields of the  $17\pi/33$ -mode thereby become much less favourable for storing energy. If necessary, it would be feasible to re-machine the copper grid so that it can host the HOM-coupler as the transition from air to vacuum is done at the level of the VPP flanges. Obviously, better results could be achieved by using more than one HOM-coupler in the lower half of the cavity. Regarding the influence of this mitigation option on the FPB, one needs to observe the overall induced frequency shift due to the total number of couplers placed inside the cavity.

### STEP 4: CHANGE OF STRUCTURE

The observations made with the VPP coupler immediately led to the question if sufficient mitigation of the  $17\pi/33$ -mode could be achieved by primarily targeting its R/Q. This requires a change of the TWS that mitigates the HOM but leaves the FPB untouched. Such a method would also be very valuable in the mitigation of the two high-R/Q modes as conventional methods of damping their Qs come to their limits. The probe of the 630 MHz coupler is already known to be resonant in the targeted frequency range and placing it directly in the honeycomb grid with good RF contact to the outer envelope as shown in Fig. 9 introduces a third resonator in the cell of the VPP. The effect of such a resonant post is most easily demonstrated by loading a long piece of the TWS envelope with a single drift-tube and stem assem-

Content from this work may be used under the terms of the CC BY 3.0 licence (© 2018). Any distribution of this work must maintain attribution to the author(s), title of the work, publisher, and DOI.

Figure 10a shows the typical HOM field profile with strong axial electric field of the stem resonator which is not supported by the bare waveguide. With the resonant post in

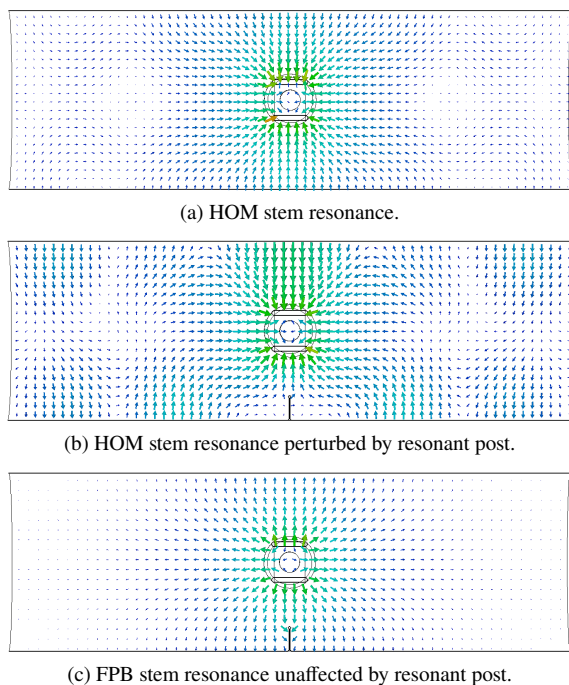


Figure 10: Electric field profiles in a long piece of circular envelope loaded by a single drift-tube and stem assembly (field magnitudes colour coded on a logarithmic scale).

place, Fig. 10b, energy can not be stored in the lower part of the cell. This will avoid that EM fields, e.g. those of the  $17\pi/33$ -mode, are pushed into the lower half of the structure making them inaccessible to the HOM-couplers. Thereby, the resonant posts act as a counter weight to the numerous couplers on top of the structure making these even more effective. In addition, the R/Q of the stem resonance calculated over the length of the cell is reduced from  $18\ \Omega$  for the unperturbed case to  $13.5\ \Omega$  for the case with the resonant post in place (a reduction by 25%). The effects described above can be explained by the fact that the displacement current picked up by the resonant post is shorted to the outer envelope of the cavity. For the case of multi-cell structures also the coupling mechanism to the neighbouring cells is partially suppressed in this manner.

The resonant posts are merely effective in cells with strong electric field and VPPs are only available in cells 3, 6 and 9 of each 11-cell section, Fig. 2. Therefore, Fig. 5 is again consulted to appropriately choose the cells or VPPs respectively on a 3-section TWS for deployment of resonant posts, with the goal to mitigate the three problematic HOMs. The impact of two resonant posts in cells 9 and 25 as marked in Fig. 1 on these modes is shown in the last row of Table 2. Not only is the  $17\pi/33$ -mode heavily mitigated but also the R/Q of the two other HOMs is significantly reduced. The achieved damping for the combination of additional and improved couplers and three resonant posts in cells 9, 17

and 25 as calculated by the CST and T3P solvers is shown in Fig. 4a. The  $14\pi/33$ -mode at 630 MHz is now heavily damped in this configuration whereas part of the impedance is shifted towards lower frequencies. It is conceivable that the complex load deployed on the HOM-coupler outputs is quite narrowband and that the couplers are therefore less effective at 626 MHz than in the range 628-630 MHz. In the case that the  $23\ \Omega$  characteristic impedance setting is used, this problem will not occur. As already mentioned, the complex load will be investigated further to achieve a more uniform damping over the 630 MHz frequency range without having to change the HOM-couplers themselves. It can however in general be noted that the HOM impedance is not only damped but also distributed to lower frequencies (this is not the case towards higher frequencies) by the new mitigation techniques, Fig. 4b.

The field profile of the accelerating FPB under the influence of a resonant post remains basically unchanged, see Fig. 10c. A frequency shift on the order of 100 kHz has however to be expected (the 200 MHz TWS is considered very broadband). It is planned to measure the frequency shift of the travelling wave FPB and the degradation of field flatness due to resonant posts in three cells on a 3-section structure in the lab as soon as it is available. It has to be evaluated if a potentially slight reduction in accelerating voltage can be accepted for a significantly improved HOM damping. First studies for optimizing the shape of the resonant electric pick-ups for their new purpose suggest that also slightly shorter posts with possibly even less impact on the FPB might be effective enough to mitigate the HOMs. The above described effects of the resonant posts on the HOMs could already be confirmed by RF lab measurements on a single section [6].

## CONCLUSION

This work showed a systematic, step-by-step improvement of today's damping scheme for longitudinal beam coupling impedance employed on the SPS 200 MHz TWSs. The complex loads for the HOM-couplers will undergo further optimization and can not only be employed on the 33- but also the 44-cell accelerating structures. The HOM-coupler placed in VPPs and the pedestal-coupler both showed good performance. Best HOM mitigation is achieved by the placement of resonant posts in selected cells, which is cost effective and requires no machining of cavity parts. This solution could even be employed without compromising the original purpose of the VPPs as the installation of a whole HOM-coupler with filter geometry is not required. The impact on the travelling-wave FPB and the accelerating voltage of all couplers, but especially the resonant posts, has however to be studied in further detail. Final optimization of damping performance will be done once one of the options is chosen for implementation.

## ACKNOWLEDGEMENTS

The authors thank F. Caspers, A. Farricker and B. Popovic from BE-RF for fruitful discussions and their input. Furthermore, this work is sponsored by the Wolfgang Gentner Programme of the German Federal Ministry of Education and Research (BMBF) and used resources of the National Energy Research Scientific Computing Center (NERSC), a U.S. Department of Energy Office of Science User Facility operated under Contract No. DE-AC02-05CH11231.

## REFERENCES

- [1] E. Shaposhnikova *et al.*, “Removing Known SPS Intensity Limitations for High Luminosity LHC Goals,” in *Proc. IPAC2016*, Busan, Korea, May 2016, pp. 989–991, 2016. doi:10.18429/JACoW-IPAC2016-M0P0Y058
- [2] G. Dôme, “The SPS acceleration system travelling wave drift-tube structure for the CERN SPS,” no. CERN-SPS-ARF-77-11, p. 26 p, May 1977. <https://cds.cern.ch/record/319440>
- [3] P. Kramer and C. Vollinger, “Proceedings of the ICFA Mini-Workshop on Impedances and Beam Instabilities,” in *CERN Yellow Reports: Conference Proceedings*, ser. CERN-2018-003-CP, V. Brancolini, G. Rumolo and S. Petracca, Ed., vol. 1/2018. Benevento, Italy: CERN, Geneva, 2017, pp. 57–62. doi:10.23732/CYRCP-2018-001
- [4] CST AG, Darmstadt, Germany, <http://www.cst.com/>
- [5] ACE3P, [https://portal.slac.stanford.edu/sites/ard\\_public/acd/](https://portal.slac.stanford.edu/sites/ard_public/acd/)
- [6] P. Kramer, Ph.D. dissertation, to be published.
- [7] A. Candel, A. Kabel, L. Lee, Z. Li, G. Ng, G. Schussman, and K. Ko, “State of the art in electromagnetic modeling for the Compact Linear Collider,” in *Proc. J. Phys.*, vol. 180, pp. 012004, 2009. doi:10.1088/1742-6596/180/1/012004
- [8] H. Padamsee, T. Hays, and J. Knobloch, *RF Superconductivity for Accelerators*, 2nd ed. Wiley, 2008.
- [9] E. Haebel, “Couplers for cavities,” in *CAS, CERN Accelerator School, Superconductivity in Particle Accelerators*, no. CERN 96-03, 1996, pp. 231–264.
- [10] W. Schminke, “Strong damping of single-cell accelerator cavities by resonant loops,” CERN, Geneva, Tech. Rep. SPS/ARF/WS/gs/81-68, 1981.